JOURNAL OF CATALYSIS **180,** 171–183 (1998)
ARTICLE NO. CA982277

Reduction of NO_x over Fe/ZSM-5 Catalysts: Adsorption Complexes and Their Reactivity toward Hydrocarbons

Hai-Ying Chen, Timur Voskoboinikov, and Wolfgang M. H. Sachtler

V.N. Ipatieff Laboratory, Center for Catalysis and Surface Science, Department of Chemistry, Northwestern University, Evanston, Illinois 60208

Received March 20, 1998; revised August 31, 1998; accepted September 3, 1998

Fe/ZSM-5 prepared via sublimation catalyzes the reduction of NO_x to N_2 in the presence of excess O_2 and H_2O. Propane, *iso*-butane, and propene are active reductants; methane is inactive. The NO_x reduction rate is negligible in the absence of O_2; it increases steeply with P_{O_2} and passes through a maximum. The equilibrium between $NO + O_2$ and NO_2 is swiftly established over a clean catalyst, but deposits impede this reaction. $NO + O_2$ forms chemisorption complexes, NO_y, with $y \geq 2$. Upon their reaction with hydrocarbon, a nitrogen-containing deposit is formed on the catalyst. It reacts with NO_2, but not with NO, releasing large quantities of N_2. N_2O seems not to be a precursor of N_2. Isotopic labeling shows that one N atom in every N_2 comes from the deposit; the other comes from NO_2. Less deposit is formed with propane, more with propene. As deposits also block catalyst sites, the rate limiting step in NO_x reduction depends on the nature of the hydrocarbon. Deposits are oxidized by O_2 and volatilized by H_2O at high temperature; these processes contribute to the relative efficiency of different hydrocarbons in NO_x reduction over Fe/ZSM-5. © 1998 Academic Press

Key Words: **DeNO$_x$; SCR of NO$_x$; Fe/ZSM-5; adsorbed nitro groups; adsorbed nitrates; reactive deposits.**

1. INTRODUCTION

Several ZSM-5-supported catalysts are active in the selective reduction of NO_x (any $NO + NO_2$ mixture) in the presence of excess oxygen. Among this group, certain Fe/ZSM-5 catalysts excel by their unique propensity to retain high activity also in the presence of a large excess of *water* vapor (1–4). This is crucial for the potential application of such catalysts in the emission of internal combustion engines, in particular under lean burn conditions. In previous papers we showed that efficient Fe/ZSM-5 catalysts can be prepared by sublimation of $FeCl_3$ vapor onto HZSM-5, followed by hydrolytic removal of chlorine (3, 4). They catalyze NO_x reduction with *iso*-butane to N_2 in the presence of 10% water at 350°C with a yield of 76%. An even higher N_2 yield, near 90%, was obtained with an improved catalyst, containing a small amount of lanthanum (5). Below the optimum temperature of 350°C the NO_x to N_2 yield over such catalysts is higher in the presence of water vapor than with a dry feed.

Little is known about the molecular reaction mechanism of NO_x reduction over Fe/ZSM-5. For Co/ZSM-5 Cowan *et al*. showed that NO_x reduction with methane displays a large kinetic isotope effect when CH_4 is replaced by CD_4, which suggests that H abstraction is rate limiting, leading to the formation of alkyl radicals (6). Previous work in this laboratory with Cu/ZSM-5 and Co/ZSM-5 had revealed that exposure of the catalysts to a mixture of $NO + O_2$ gives rise to the formation of characteristic chemisorption complexes, NO_y, which are able to chemically interact with alkanes (7). Assuming that propyl radicals are formed from propane, it has been proposed that such radicals react with NO to form first nitrosopropane, which could isomerize to an oxime. Adsorbed oximes have been shown to react with NO molecules, yielding N_2 and N_2O (8). When the N atom in the oxime was the isotope ^{14}N, but ^{15}NO was used in the feed gas, the product consisted mainly of isotopically mixed molecules $^{14}N^{15}N$ and $^{14}N^{15}NO$ (8). The labeling data exclude the hypothesis that a nitrogen-free hydrocarbonaceous overlayer on the catalyst is the actual reductant for NO_x (9). If deposits are active, they should expose nitrogen–containing groups and N_2 would have to be formed by their interaction with NO_2.

For Cu/ZSM-5 and Co/ZSM-5, a major role of the metal ions appears to direct $NO + O_2$ toward forming a metal-specific type of adsorption complex, NO_y. With Cu/ZSM-5, FTIR studies showed bands that were assigned to nitro groups, monodentate and bidentate nitrate ions. In contrast, with Co/ZSM-5 the reactive NO_y complex displays IR bands assigned to the nitrito group Co–O–N=O. It appears to be able to abstract H atoms even from methane (7).

In the present work, a similar research strategy has been applied to Fe/ZSM-5 catalysts, prepared by our sublimation method. First, the role of oxygen has been examined by comparing temperature-programmed desorption (TPD) profiles of Fe/ZSM-5 samples that were exposed to either NO or a mixture of $NO + O_2$. FTIR is used to identify adsorption complexes and their reactivity toward hydrocarbons. In this context a comparison of propane and *iso*-butane is relevant because the radical formation concept predicts that H abstraction should be easier when a *tertiary*

0021-9517/98 $25.00

iso-C_4 radical is formed. The formation of N_2 upon exposure of the NO_y complexes to alkanes is monitored by mass spectrometry. There are indications that deposits are formed in this interaction, and these deposits have again been exposed to NO and NO_2. Isotopic labeling is used to identify the processes where N_2 and N_2O molecules are produced. Comparison of these results with the overall performance in conventional catalytic tests has been used to identify secondary factors affecting measured activities, such as site blocking by reaction products or coke.

2. EXPERIMENTAL

2.1. Catalyst Preparation

Fe/ZSM-5 catalysts were prepared by chemical vapor deposition (3, 4). Na/ZSM-5 (UOP lot# 13923-60, Si/Al = 14.2, Na/Al = 0.67) was first transformed to H/ZSM-5 by ion exchange with a dilute $NH_4 \cdot NO_3$ solution, followed by calcination in an O_2 flow at 550°C for 4 h. Anhydrous $FeCl_3$ (Aldrich, 97%) was sublimed into H/ZSM-5, where it reacts with zeolite protons

$$H^+ + FeCl_3 = [FeCl_2]^+ + HCl\uparrow \qquad [1]$$

until all protons are replaced by $[FeCl_2]^+$. After washing with doubly deionized H_2O to remove chlorine and drying in air, the sample was calcined in flowing O_2 at 550°C for 2 h. Elemental analysis by inductively coupled plasma atomic emission shows that the Fe/Al ratio in Fe/ZSM-5 is unity. Characterization data of such catalysts have been published elsewhere (4).

2.2. Reaction Studies

Catalytic tests were carried out in a continuous flow reactor (4). A 0.200-g Fe/ZSM-5 sample was charged in a quartz reactor with a porous frit. The gas flow rate was regulated by mass flow controllers, and the total flow rate was maintained at 280 mL/min. The inlet feed composition was 0.2% NO, 3% O_2, and 0.8% carbon flux (0.2% for *i*-C_4H_{10}, 0.27% for C_3H_8 or C_3H_6, 0.8% for CH_4), with He used as a diluent. When desired, 10% H_2O was added by a water saturator. To avoid condensation of water, the whole line was heated with heating tape. The reaction temperature was increased stepwise from 200 to 500°C. The catalyst was preconditioned at each temperature for 30 min before products were analyzed by GC-TCD with Alltech 13X molecular sieve and Parapak Q columns.

2.3. Temperature-Programmed Oxidation

After testing an Fe/ZSM-5 catalyst for 3 h in the microflow reactor for SCR of NO_x with a given hydrocarbon at 300°C, the reactor was cooled to RT under a hydrocarbon-free gas flow. The reactor was then sealed and attached to a temperature-programmed system equipped with a Dycor Quadrupole Gas Analyzer mass spectrometer (TP-MS) (10). Temperature-programmed oxidation (TPO) was done with a 5% O_2/Ar flow of 60 mL/min and a temperature ramp of 8°C/min.

2.4. Adsorption and Desorption Studies

All measurements were carried out on a TP-MS system with a quartz reactor charged with 0.200 g of Fe/ZSM-5 on a porous frit. The samples were first heated in 60 mL/min 5% O_2/Ar flow from 24°C to 600°C with a 8°C/min ramp, followed by cooling to RT in the same gas flow. The samples were subsequently purged with a UHP He flow at 60 mL/min for 0.5 h. Adsorption was measured with a mixture of NO (0.7%) in He (for "NO only"), or NO (0.7%) + O_2 (6%) in He (for "NO + O_2") at a flow rate of 60 mL/min. This mixed gas flow was first bypassed to get a background signal. The changes of the MS peak intensities were monitored at an adsorption temperature of 24°C. Once equilibrium was established again, the gas flow was switched back to UHP He at 60 mL/min and the catalyst was purged for 1 h. A TPD profile was then registered in the same flow while the temperature was increased from 24 to 600°C at 8°C/min.

2.5. FTIR Measurements

Spectra were collected on a Nicolet 60SX FTIR spectrometer equipped with a liquid N_2-cooled MCT detector. An Fe/ZSM-5 sample was pressed into a self-supporting wafer of 8–10 mg/cm^2 and placed into a Pyrex glass cell sealed with NaCl windows. The sample was calcined *in situ* to 500°C in an O_2/He (5%) flow of 100 mL/min and then cooled to 200°C under the same flow. In the following experiments the temperature was held at 200°C. For NO + O_2 adsorption, a gas mixture of NO (0.5%) + O_2 (3%) + He at a total flow rate of 100 mL/min was passed through the cell for 30 min, followed by purging with O_2 (3%) + He 100 mL/min for 30 min. To probe for reactivity of the adsorbed species, a mixture of C_3H_8 or *i*-C_4H_{10} (0.2%) + O_2 (3%) + He 100 mL/min was introduced into the cell. *In situ* reaction measurements were carried out at 200°C under a flow of the same gas mixture to which 0.5% NO was added. All spectra were taken at 200°C, accumulating 50 scans with a spectral resolution of 1 cm^{-1}. The gas inside the cell immediately after scanning a sample was used as the spectroscopic background. All spectra shown in this paper were normalized by subtracting the spectrum of the calcined sample from the actual spectrum measured under flow conditions.

2.6. Mass Spectrometry

A recirculating manifold equipped with a Dycor Quadrupole Gas Analyzer was used to analyze the released gases.

A 0.400-g Fe/ZSM-5 catalyst was charged in a Pyrex reactor which was attached to this system. Prior to the experiment, the catalyst was calcined to 500°C in an O_2 (UHP) flow of 100 mL/min and cooled to 200°C. With the catalyst held at this temperature, the system was pumped (background pressure 10^{-3} Torr) for 0.5 h before a dosed gas mixture was admitted to the sample loop and circulated over the catalyst. Signal intensities were normalized using the Ar^{2+} peak ($M/e = 20$) as an internal standard.

3. RESULTS

3.1. Effect of O_2 Concentration on Catalytic Activity

With Cu/ZSM-5 and other zeolite supported lean burn deNO_x catalysts it is well known that the selectivity toward N_2 is enhanced by the presence of O_2 in the feed gas (11, 12). Previously, we had reported on the SCR activity of our Fe/ZSM-5 catalysts at constant O_2 pressure while varying the temperature (4). A maximum N_2 yield of about 76% was found near 350°C with a feed of 0.2% NO + 0.2% *i*-C_4H_{10} + 3% O_2. In Fig. 1, the N_2 yield at 350°C is plotted against the partial pressure of O_2, while the other parameters are kept constant. In the absence of O_2, NO reduction at 350°C was negligible; it steeply increases with P_{O_2}, reaching an N_2 yield of 54% for 0.5% O_2. Further increase of the N_2 yield is slower, and a maximum is reached for 2% O_2; this is followed by a slow decrease. The O_2 content required for the stoichiometric reaction

$$i\text{-}C_4H_{10} + NO + 6O_2 = 4CO_2 + 1/2N_2 + 5H_2O \quad [2]$$

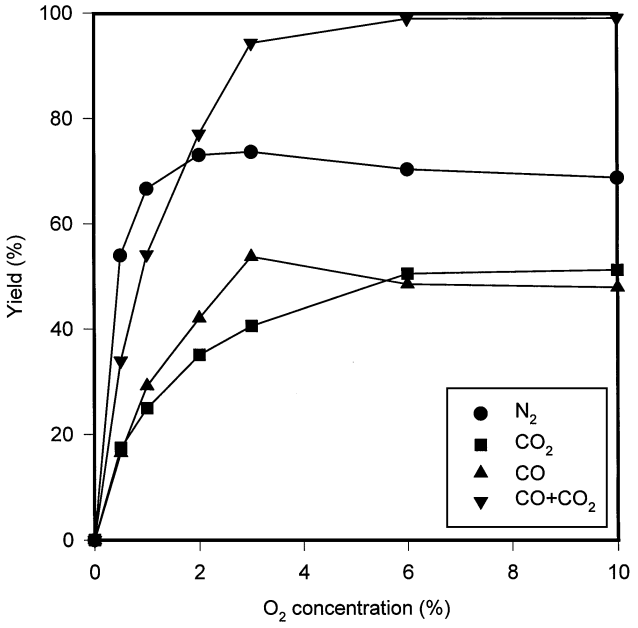

FIG. 1. The effect of oxygen concentration on the catalytic activity of Fe/ZSM-5 Reaction conditions: 0.200 g Fe/ZSM-5, 0.2% NO, 0.2% *i*-C_4H_{10}, 280 mL/min, 350°C.

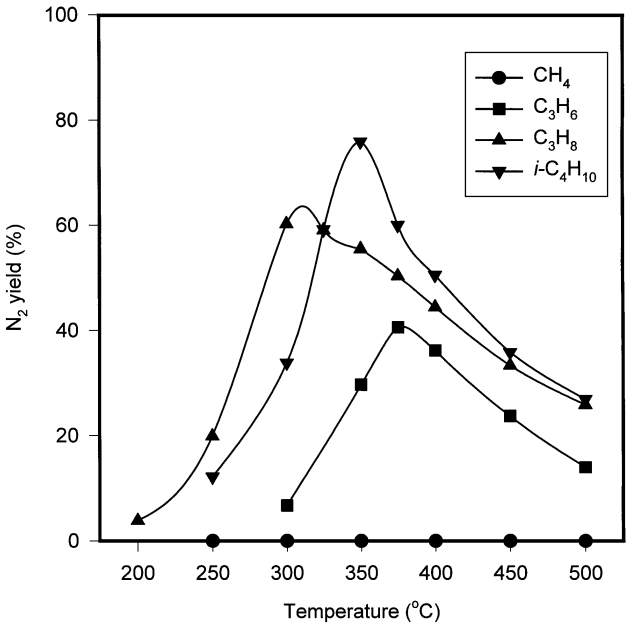

FIG. 2. Temperature dependence of N_2 yield over Fe/ZSM-5 with different hydrocarbons Reaction conditions: 0.200 g Fe/ZSM-5, 0.2% NO, 3% O_2, 0.2% *i*-C_4H_{10} (0.8% CH_4, 0.27% C_3H_8 or C_3H_6), 280 mL/min.

would be 1.2%. Beyond the maximum, the combustion activity of the hydrocarbon increases and part of the primary product CO is oxidized to CO_2. These results are similar to those reported over Cu/ZSM-5 (13–15), but there are also remarkable differences:

(i) more CO is formed over Fe/ZSM-5 than over Cu/ZSM-5;

(ii) the decrease in N_2 yield for oxygen concentrations beyond the maximum is steeper over Cu/ZSM-5 than over Fe/ZSM-5.

3.2. NO_x Reduction with Different Hydrocarbons

The selective catalytic reduction of NO_x over Fe/ZSM-5 has been tested with CH_4, C_3H_6, C_3H_8, and *iso*-C_4H_{10}, always using the same carbon flux. Figure 2 shows the N_2 yield as a function of reaction temperature. With CH_4, the N_2 yield is negligible in the whole temperature region. Among the other hydrocarbons, C_3H_6 shows the lowest N_2 yield, but the ranking of C_3H_8 and *iso*-C_4H_{10} depends on the temperature. Below the temperature of maximum yield, *iso*-C_4H_{10}, which is the most active reductant over Cu/ZSM-5 (13), shows a lower N_2 yield than C_3H_8. This unusual ranking at low temperature is due to the formation of deposits, which were characterized by TPO (not shown). With C_3H_8 as a reductant, there is virtually no deposit on the catalyst. With *iso*-C_4H_{10}, and even more so with C_3H_6, large amounts of carbonaceous deposits are detected. The CO_2 peak areas are 1.1 and 3.4×10^{-4} mol per gram of catalyst for *iso*-C_4H_{10} and C_3H_6, respectively.

TABLE 1

N_2 Yield (%) over Fe/ZSM-5 at Various Temperatures under Different Conditions

C_xH_y	NO_x	H_2O	200°C	250°C	300°C	325°C	350°C	375°C	400°C	450°C	500°C
i-C_4H_{10}	NO	0		12.1	33.8	59.2	75.9	60.1	50.6	35.9	26.9
	NO_2	0	16.7	22.2	40.7	74.0	80.4	68.5	60.5	43.0	31.2
	NO	10%		18.1	49.7	70.4	76.6	59.0	50.5	36.3	28.1
C_3H_8	NO	0	3.9	19.9	60.3	59.1	55.5	50.4	44.4	33.3	25.8
	NO_2	0	3.6	21.6	66.3	65.1	57.7	50.1	43.6	32.5	26.2
	NO	10%	2.1	6.2	33.3	43.9	44.2	42.0	37.6	29.4	22.5

Note. Reaction conditions: catalyst 0.200 g; NO_x 0.2%; O_2 3%; *i*-C_4H_{10} 0.2% (or C_3H_8 0.27%); H_2O 0% or 10%; feed rate 280 mL/min.

With C_3H_8 or *iso*-C_4H_{10} the catalytic activity of Fe/ZSM-5 was also tested using NO_2 instead of NO, and in the presence of 10% H_2O. The results are compiled in Table 1, where the N_2 yield is used for ranking the catalytic activities. As reported previously (4, 5), the presence of H_2O increases the N_2 yield at low temperature when *i*-C_4H_{10} was used, but with C_3H_8 it slightly lowers the N_2 yield. With C_3H_8, almost the same activity is found with NO_2 or NO. This is not the case for *iso*-C_4H_{10}; with that reductant the N_2 yield is higher with NO_2.

3.3. *NO, NO + O_2 Adsorption, and TPD*

To understand the effect of O_2 on the catalytic activity, NO or NO + O_2 adsorption and TPD experiments were carried out over the Fe/ZSM-5. Figure 3 shows the NO adsorption profile over Fe/ZSM-5. Upon exposing the catalyst to a He flow containing 0.7% of NO, saturation is reached within ~2 min, after which time the signal intensity returns to its original value. After purging with He at room temperature and heating, NO is desorbed; the TPD profile is shown in Fig. 4. Only a low-temperature NO desorption peak with $M/e = 30$ was observed. This is mainly due to desorption of NO from the zeolite framework (10, 16–18). No desorption peak was observed for $M/e = 32$ (O_2) or $M/e = 46$ (NO_2), which indicates absence of dissociation and disproportionation for this adsorption of "NO only."

Different results are observed upon exposing Fe/ZSM-5 to a flow containing 0.7% NO and 6% O_2. Figure 5 shows the NO + O_2 adsorption profile. A very low concentration of NO_2 was observed even when the catalyst was bypassed, showing that the metal walls of the ducts catalyze a detectable reaction even at RT. However, much larger amounts of NO_2 ($M/e = 46$) were detected when the gas mixture flowed over the catalyst. For NO ($M/e = 30$), saturation was reached after 30 min exposure time, while the $M/e = 46$ peak was still increasing. During purging at room

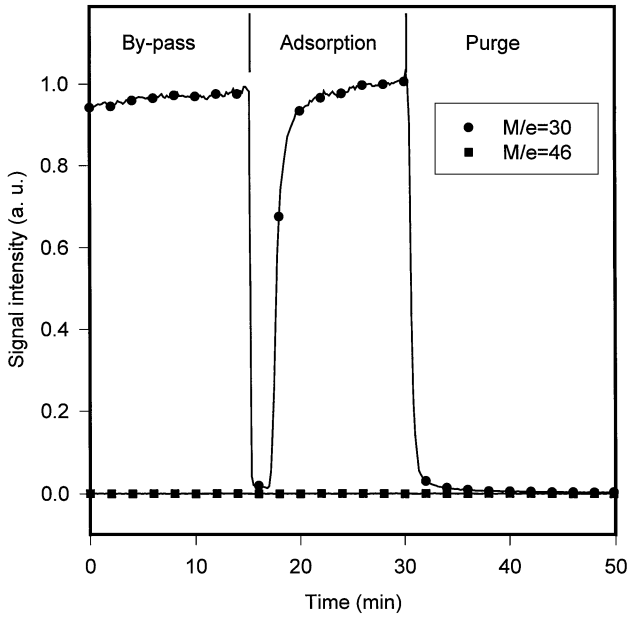

FIG. 3. Time dependence of $M/e = 30$ and $M/e = 46$ signal intensity upon exposing "NO only" over Fe/ZSM-5 catalyst at 24°C.

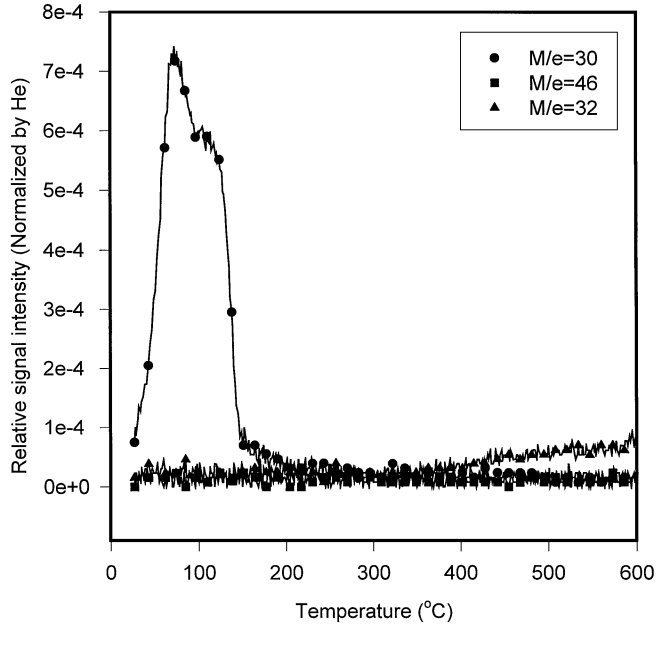

FIG. 4. TPD from Fe/ZSM-5 catalyst following "NO only" adsorption at 24°C.

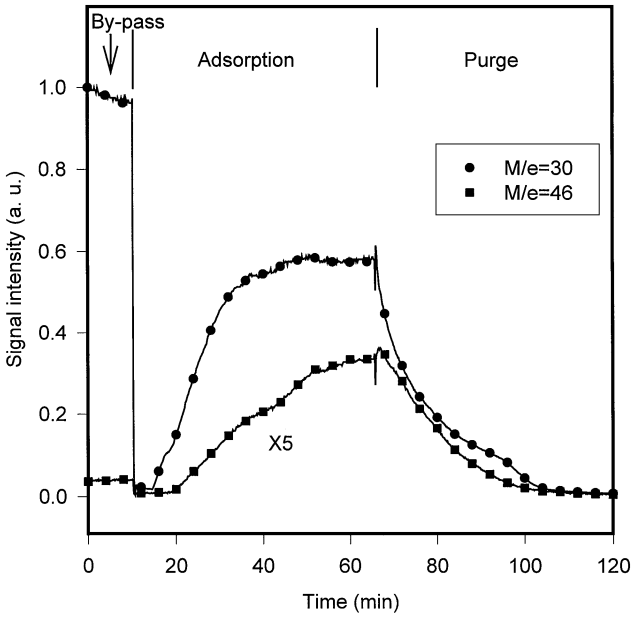

FIG. 5. Time dependence of $M/e = 30$ and $M/e = 46$ signal intensity upon exposing "$NO + O_2$" over Fe/ZSM-5 catalyst at 24°C.

temperature, both peaks decreased much more slowly than in the case of NO only. During that period, the intensity ratio of the peaks at $M/e = 46$ and $M/e = 30$ increased, which suggests that NO_2 is more strongly adsorbed. Clearly, Fe/ZSM-5 catalyzes the oxidation of NO to NO_2:

$$NO + 1/2O_2 = NO_2. \qquad [3]$$

The slow return to the baseline suggests formation of N_2O_3 and/or N_2O_4, which decompose to NO and NO_2 during desorption.

The TPD profile following adsorption of $NO + O_2$ is presented in Fig. 6. A peak with mass $M/e = 30$ at low temperature is reminiscent of the peak in Fig. 3, but its height and area are much larger. This peak is due to the sum of the parent mass of NO and the $M/e = 30$ fragment of NO_2, as it is well known that NO_2 will decompose to NO inside the ionization chamber of the mass spectrometer (19). Under the $M/e = 30$ peak, small peaks appear for $M/e = 32$ (O_2) and $M/e = 46$ (NO_2). A second family of TPD peaks for all these masses is registered at ~300°C. However, their shapes and T_{max} values are different from each other. The peak of $M/e = 46$ (NO_2) is rather symmetric with a $T_{max} = 306$°C, while the $M/e = 30$ peak is tailed with a $T_{max} = 297$°C. Comparison with mass spectra of fairly pure NO_2 suggests that the $M/e = 30$ signal is not entirely due to a fragment of the $M/e = 46$ parent, but part of it is the parent mass of NO molecules desorbed from the catalyst.

Upon exposing the catalyst to NO_2, the subsequent TPD profile is identical to that shown in Fig. 6 after adsorption of $NO + O_2$. Apparently, the same NO_y adsorption complexes are obtained in both cases.

3.4. *Identification of Adsorption Complexes and Catalyst Deposits by FTIR*

3.4.1. Adsorption of $NO + O_2$. The adsorption complexes formed upon exposing the catalyst to $NO + O_2$ at 200°C were examined by FTIR spectroscopy. This temperature was chosen to exclude weak adsorption complexes. Figures 7a–7c show the spectra for different exposure times to the $NO + O_2$ flow. Four bands are visible at 2131, 1878, 1625, and 1570 cm^{-1}. The band at 2131 cm^{-1} has been assigned to the N–O stretching vibration of NO_2^+ adsorbed on the Brønsted acid sites of the zeolite (20–23). Most recently, it was reassigned to NO^+ occupying Brønsted acid sites in the zeolite (24). Its intensity is very low and reaches saturation quickly, in accordance with our previous finding that the concentration of Brønsted sites on this catalyst is very low (4). The band at 1878 cm^{-1} has been assigned to the iron mononitrosyl complex formed by the interaction of NO with iron (25–27). Since the vibration frequency is about the same as for gas phase NO (1880 cm^{-1} (28)), the interaction of Fe with this ligand should be very weak. The bands at 1625 and 1570 cm^{-1} cannot be assigned with certainty at present, because it is impossible to study the entire spectral region. The frequency of the 1625 cm^{-1} band is very near the asymmetric stretching frequency of gaseous NO_2 (1610 cm^{-1} (28)). We tentatively assign it to a nitro group ligated to an iron ion (7, 25, 29). The band at 1570 cm^{-1} can be assigned to a nitrate group on an iron site (25, 30). For the time being, we shall use the term "nitro/nitrate groups" for both bands. The intensity of the bands at 1878, 1625, and 1570 cm^{-1} changed with increasing exposure time; the

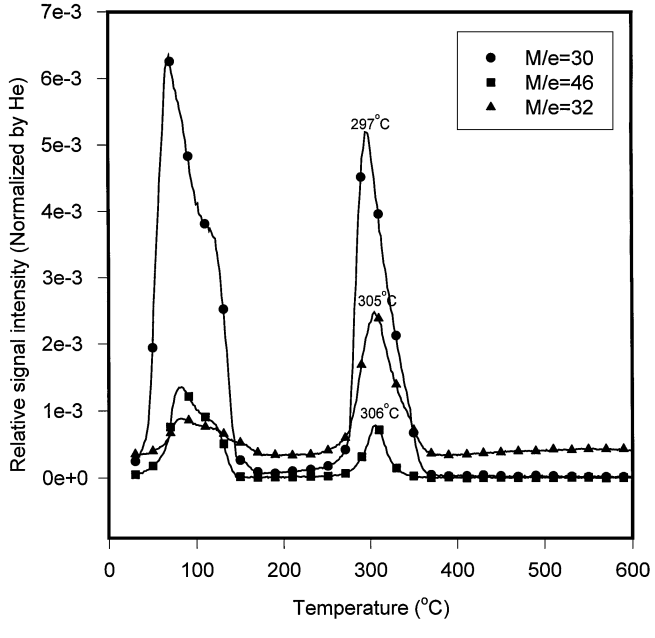

FIG. 6. TPD from Fe/ZSM-5 catalyst following "$NO + O_2$" adsorption at 24°C.

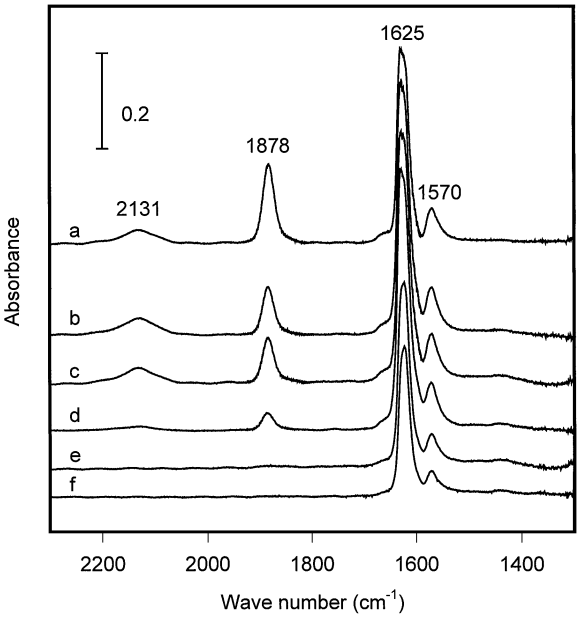

FIG. 7. FTIR spectra taken at 200°C of NO_y adsorbed Fe/ZSM-5 sample under a flow of 0.5% NO + 3% O_2 + He for 5 min (a), 15 min (b), 30 min (c); followed by purge with 3% O_2 + He for 5 min (d), 15 min (e), 30 min (f).

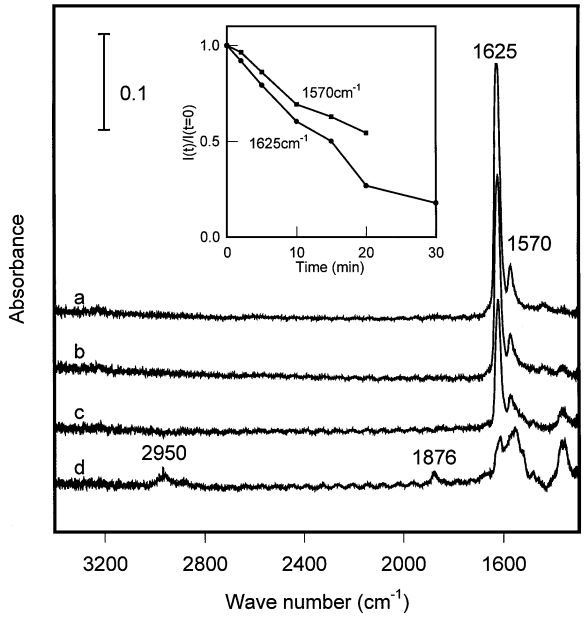

FIG. 8. FTIR spectra taken at 200°C after NO + O_2 adsorption and purge with O_2/He (a), subsequently exposed to a flow of 0.2% C_3H_8 + 3% O_2 + He flow for 5 min (b), 15 min (c), and 30 min (d). The inset depicts a plot of the band relative intensities at 1625 and 1570 cm^{-1} as a function of time.

band at 1878 cm^{-1} decreased, while the bands at 1625 and 1570 cm^{-1} increased. This could indicate that mononitrosyl and nitro/nitrate groups are adsorbed at the same iron site. When the catalyst is first exposed to the NO + O_2 flow, the NO_2 concentration is very low, so that NO will be adsorbed. Once NO is oxidized to the more strongly adsorbed nitro/nitrate groups, the intensity of the NO band will decrease while that of the nitro/nitrate groups will increase.

Figures 7d–7f show the stability of the adsorption bands upon purging with O_2/He at 200°C. In contrast, the bands at 2131 and 1878 cm^{-1} get weaker and vanish after 15 min of purging. Obviously, NO^+ and NO are weakly adsorbed. The intensity of the bands at 1625 and 1570 cm^{-1} also decreases somewhat, but does not vanish even after 30 min of purging, indicating that the nitro/nitrate groups are fairly strongly adsorbed.

3.4.2. Reactivity of the nitro/nitrate groups toward hydrocarbons. Whereas Fig. 7 illustrates the *thermal* stability of the adsorption complexes, the spectra in Fig. 8 show their *chemical reactivity* toward propane. Clearly, the nitro/nitrate groups interact chemically with propane at 200°C. A plot of the band intensities, which were measured as peak heights and normalized by their initial intensities, as a function of time is shown in the same figure. After 30 min, the band intensity has dropped to a very low level, and new bands appear in the 1700–1300 cm^{-1} region. In the C–H stretching region, a weak broad band appears at 2950 cm^{-1}. Another weak band at 1876 cm^{-1} might be assigned to a mononitrosyl complex (see below).

Figure 9 shows the reactivity of the adsorbed nitro/nitrate groups toward *iso*-butane. Clearly, this hydrocarbon reacts vigorously with these groups. Already after 5 min, both bands have decreased dramatically. A band at 1876 cm^{-1}

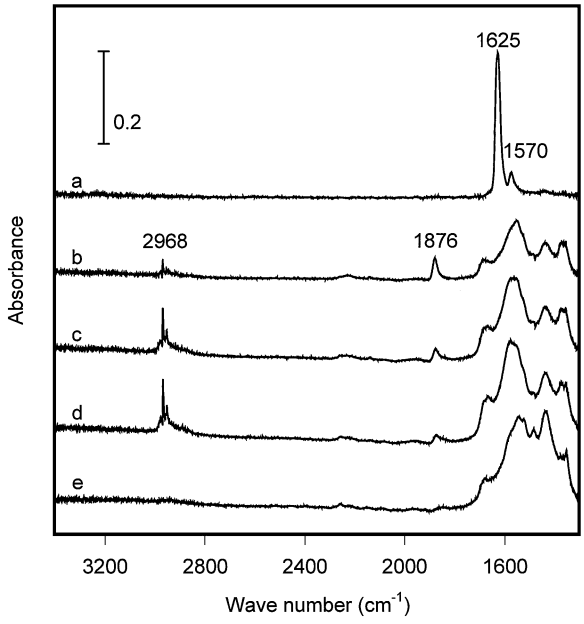

FIG. 9. FTIR spectra taken at 200°C after NO + O_2 adsorption and purge with O_2/He (a), subsequently exposed to a flow of 0.2% *i*-C_4H_{10} + 3% O_2 + He flow for 5 min (b), 15 min (c), 30 min (d), off *i*-C_4H_{10}, with a flow of 3% O_2 + He for 30 min (e).

appears immediately when *iso*-butane is introduced. Its intensity decreases with time. As its frequency is the same as that of adsorbed NO, it is possible that the reduction of the nitro/nitrate groups regenerates the mononitrosyl complex. After more extended exposure to *iso*-butane, a rather complicated set of bands appear in the 1700–1300 cm^{-1} region; they are indicative for the formation of some polymeric deposit on the catalyst. At 2968 cm^{-1}, a C–H stretching vibration appears which can be attributed to adsorbed *iso*-butane. This band disappears after successive purging with O_2/He (Fig. 9e). In contrast, the bands at low frequencies are still present basically retaining their intensity. Apparently, the deposit is more stable than the species responsible for the 2968 cm^{-1} band.

Although the deposit is rather stable against O_2/He flow at 200°C, it displays a remarkable reactivity toward NO_2 (or $NO + O_2$) as shown by the three spectra in Fig. 10. Feature (a) was registered after reaction of NO_y with *iso*-C_4H_{10}, followed by purging with He at 200°C. The band at 1878 cm^{-1} that might be due to mononitrosyl complex is still visible, which suggests that it is thermally stable. This increased thermal stability of the mononitrosyl complex in comparison to that in Fig. 7 is assumed to be caused by a partial reduction of the iron from Fe^{3+} to Fe^{2+} by the hydrocarbon. It is known that this reduction does not change the position of the 1876 cm^{-1} band, but NO is ligated more strongly to Fe^{2+} than to Fe^{3+} (31, 32). Bands in the 1700–1300 cm^{-1} region are due to a polymeric deposit. Remarkably, their intensity decreases upon exposure to the

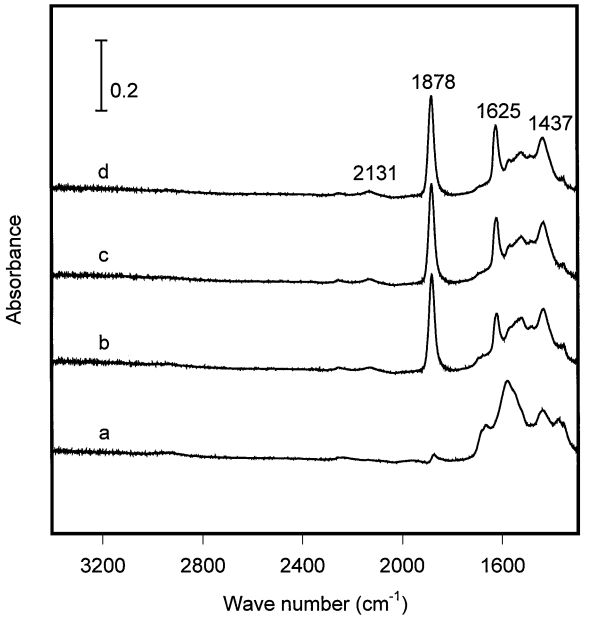

FIG. 10. FTIR spectra taken at 200°C after exposing a NO_y adsorbed sample to a flow of 0.2% *i*-C_4H_{10} + 3% O_2 + He for 0.5 h, followed by purge with He for 30 min (a), subsequently exposed to a flow of 0.5% NO + 3% O_2 + He for 5 min (b), 15 min (c), and 30 min (d).

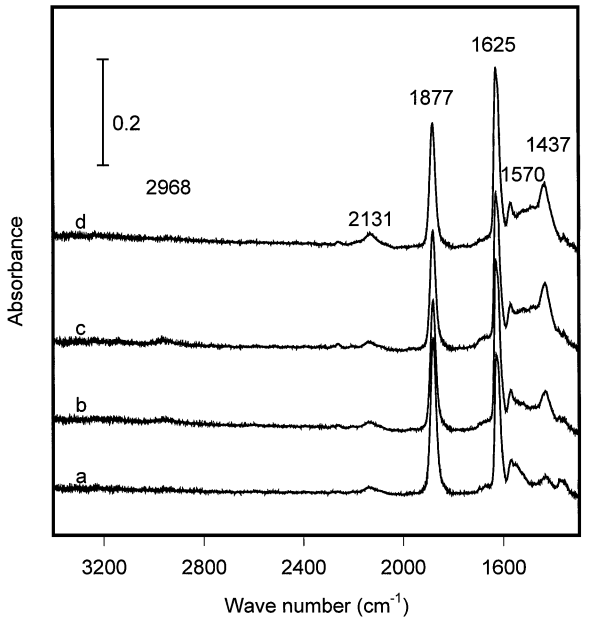

FIG. 11. FTIR spectra taken at 200°C under a flow of 0.2% C_3H_8 + 0.5% NO + 3% O_2 + He flow for 5 min (a), 15 min (b), 30 min (c), subsequently under a flow of 0.5% NO + 3% O_2 + He for 30 min (d).

$NO + O_2$ flow. Meanwhile, some carbonate (bands 1437, 1357 cm^{-1}) was formed on the catalyst. In addition to the mononitrosyl complex, other features are observed. As in Fig. 7, they include NO^+ and nitro/nitrate groups.

3.4.3. FTIR spectra under $C_xH_y + NO + O_2$ flow. Figure 11 shows the FTIR spectra registered *in situ* under a flow of $C_3H_8 + NO + O_2$ at 200°C. The bands at 2131, 1877, 1625, and 1570 cm^{-1}, shown in Fig. 7 under $NO + O_2$, are again observed. However, the intensity of the 1877 cm^{-1} band is higher, while that of the 1625 and 1570 cm^{-1} bands is lower. Clearly, the nitro/nitrate groups react with propane. Some new bands appear during reaction in the region of 1700–1300 cm^{-1}, which is due to the formation of carbonate and carbonaceous deposits. However, their intensity is low.

Figure 12 shows the FTIR spectra under a flow of *iso*-$C_4H_{10} + NO + O_2$ at 200°C. Replacing propane by *iso*-butane causes rather remarkable changes. The 1876 cm^{-1} band, assigned to a mononitrosyl complex, is only visible in the initial stage of exposing the catalyst to this gas. It is difficult to distinguish the bands at 1625 and 1570 cm^{-1}, which are assigned to nitro/nitrate groups, from the complicated absorption bands of the deposit in the 1700–1300 cm^{-1} region. These increase rapidly with time. Meanwhile, a broad band emerges at 3145 cm^{-1}; this can be assigned to a C–H stretching vibration of an unsaturated compound. Assignment of this band to an O–H stretching and/or an N–H stretching vibration is also possible (33). Also, the C–H stretching vibration at 2967 cm^{-1}, assigned to adsorbed *iso*-butane, is visible. In the region of 2300–2100 cm^{-1}, a band at 2255 cm^{-1} appeared immediately upon exposing the

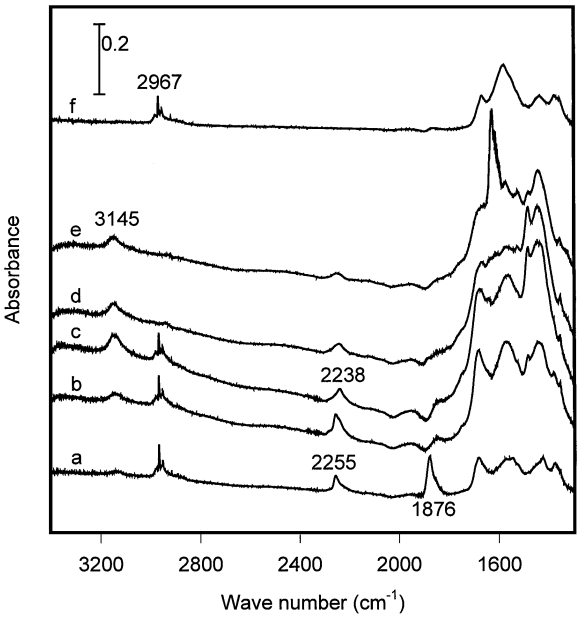

FIG. 12. FTIR spectra taken at 200°C under a flow of 0.2% *i*-C_4H_{10} + 0.5% NO + 3% O_2 + He flow for 5 min (a), 15 min (b), 30 min (c), subsequently under a flow of 0.5% NO + 3% O_2 + He for 30 min (d), following (c) under a flow of 0.5% NO_2 + 3% O_2 + He for 30 min (e), calcined sample under a flow of 0.2% *i*-C_4H_{10} + 3% O_2 + He flow for 30 min (f).

catalyst to the gas mixture. Its intensity reached a maximum and then decreased with exposure time. Another band at 2238 cm^{-1} continued to grow. Bands in this region can be ascribed to an $X{=}Y{=}Z$ and/or an $X{\equiv}Y$ stretching vibration. It has been reported that organic nitriles, cyanates, and/or isocyanates are potential intermediates of SCR of NO with hydrocarbons (34–41). It is clear from Fig. 12 that a deposit is formed on the Fe/ZSM-5 catalyst and that its quantity is larger upon exposure to *iso*-C_4H_{10} + NO + O_2 than if NO is *not* present in the gas (Figs. 12c and 12f). This deposit appears to block sites for NO adsorption. Thus, reaction (3) that is catalyzed by the iron sites will be hindered. This deposit is not very reactive towards NO + O_2 when the rate of reaction (3) is negligible, as can be seen from Fig. 12d. After 30 min of flowing NO + O_2 over the partially covered Fe/ZSM-5 catalyst, the band attributed to *iso*-butane disappears, while bands attributed to polymeric deposits decrease only insignificantly. However, this deposit reacts more quickly with NO_2 + O_2 flow, as shown in Fig. 12e. Under the same conditions, the intensity of the bands corresponding to the deposits decreases more severely when NO is replaced by NO_2. This result confirms that the catalytic oxidation of NO to NO_2 is suppressed by the deposit.

3.5. Identification of Reaction Steps by Mass Spectrometry

While the FTIR results show that the nitro/nitrate groups react with C_3 and C_4 hydrocarbons, they do not provide information on the gas phase products of this interaction. Mass spectrometry was therefore used to analyze the released gas. In order to distinguish $^{14}N_2$ and CO, $^{14}N_2O$ and CO_2, the labeled molecule ^{15}NO was used in this part of the work. This led to some surprising observations.

First, calcined Fe/ZSM-5 catalysts were exposed to a circulating gas mixture of 10 Torr ^{15}NO + 80 Torr O_2 + 10 Torr Ar for 1 h, followed by evacuation for 0.5 h. These samples, now loaded with nitro/nitrate groups, were subsequently exposed at 200°C to a circulating mixture of 10 Torr hydrocarbon, 80 Torr O_2, and 10 Torr Ar (used as internal standard). With one sample the hydrocarbon was propane; with the other it was *iso*-butane. With propane, a small amount of N_2 and N_2O was released when the hydrocarbon contacted the NO_y-loaded catalyst. Figure 13 shows the relative signal intensity of $^{15}N_2$ ($M/e = 30$) and $^{15}N_2O$ ($M/e = 46$) as a function of time. Clearly, propane reacts with the NO_y species, consistent with the FTIR results shown in Fig. 8. Initially, the signal intensity increased quite steeply, later leveling off. This "level-off" was not due to the lack of hydrocarbon, as the intensity of signal $M/e = 29$ (fragment of C_3H_8) was still rather high and that of $M/e = 44$ (CO_2) was still increasing (not shown). Upon using *iso*-C_4H_{10} instead of C_3H_8, neither the $^{15}N_2$ nor the $^{15}N_2O$ signal intensity changed much, although the FTIR data in Fig. 9 show that *iso*-C_4H_{10} reacts swiftly with the NO_y. It is possible that this quick reaction leads to nitrogen-containing organic compounds, which are strongly adsorbed on the catalyst.

The above samples, which had almost the same history except that one catalyst had been contacted with propane and the other with *iso*-butane, were then evacuated for 0.5 h

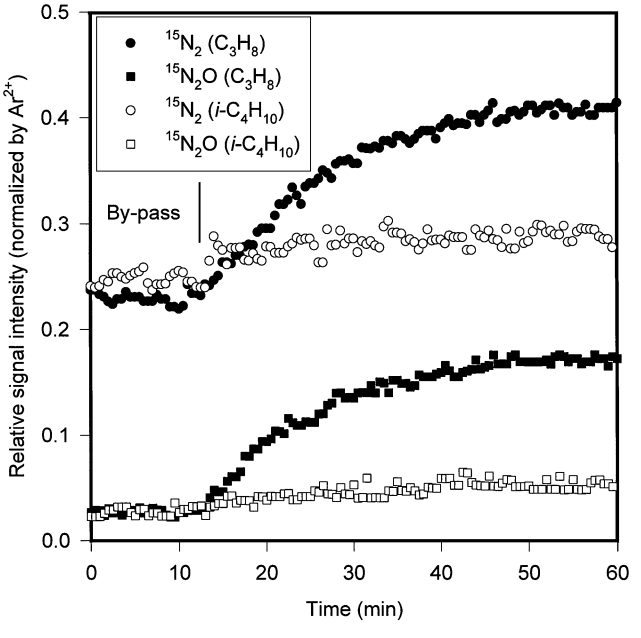

FIG. 13. Time dependence of the relative signal intensity upon circulating a mixture of 10 Torr C_3H_8 (or *i*-C_4H_{10}) + 80 Torr O_2 + 10 Torr Ar over an NO_y-adsorbed Fe/ZSM-5 sample.

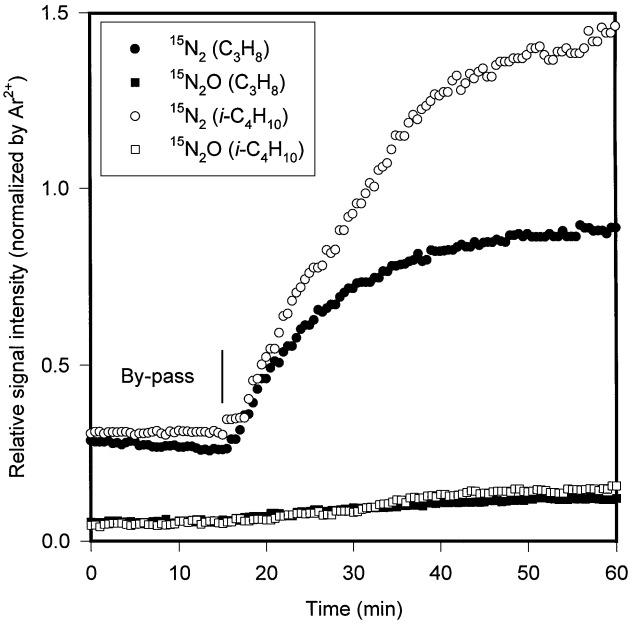

FIG. 14. Time dependence of the relative signal intensity upon circulating a mixture of 10 Torr NO + 80 Torr O_2 + 10 Torr Ar over an Fe/ZSM-5 sample, on which a nitrogen-containing deposit has been formed with C_3H_8 or i-C_4H_{10}.

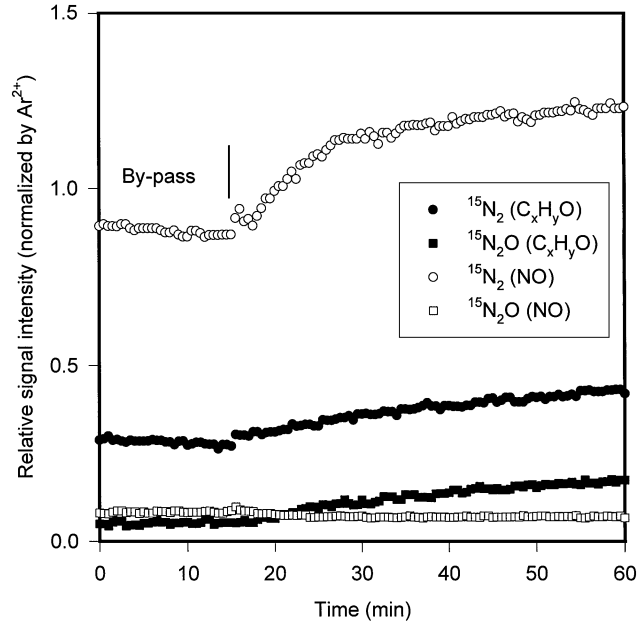

FIG. 15. Time dependence of the relative signal intensity: Solid symbols—upon circulating a mixture of 10 Torr NO + 80 Torr O_2 + 10 Torr Ar over an Fe/ZSM-5 sample, on which a C_xH_yO deposit has been formed with i-C_4H_{10} + O_2; open symbols—upon circulating a mixture of 10 Torr NO + 10 Torr Ar over an Fe/ZSM-5 sample, on which a nitrogen-containing deposit has been formed with i-C_4H_{10}.

and exposed to a circulating mixture of 10 Torr ^{15}NO + 80 Torr O_2 + 10 Torr Ar. As shown in Fig. 14, this reaction of NO_x gave rise to gas evolution: a large amount of $^{15}N_2$ and some $^{15}N_2O$ are formed in both cases. The amount of $^{15}N_2$ is larger with the sample that was previously exposed to *iso*-C_4H_{10}. Remember that FTIR had also shown more deposit formation with *iso*-C_4H_{10} than with C_3H_8.

This result triggers the question of whether the carbonaceous deposit merely acts as a reductant for impinging NO or NO_2, as has been proposed previously (9). To check this, we created a deposit by contacting a mixture of 10 Torr *iso*-C_4H_{10} + 80 Torr O_2 + 10 Torr Ar with a freshly calcined Fe/ZSM-5 catalyst and exposed it, after evacuation, to the same recirculating NO_x-containing mixture. As shown in Fig. 15 (solid symbols), very little $^{15}N_2$ was formed in this case; however, some $^{15}N_2O$ is formed, the amount of which is comparable to that in Fig. 14.

It thus seems that for N_2 evolution from the reaction of a deposit with NO_x, the deposit must be formed from adsorbed NO_y groups. In order to clarify whether nitrogen-containing groups of the deposit are directly involved in the formation of N_2, the following experiment using labeled nitrogen was carried out. First a deposit was laid down by the procedure mentioned above, using ^{14}NO for the preparation of the NO_y groups. This deposit-laden sample was then exposed to a circulating mixture of 10 Torr ^{15}NO + 80 Torr O_2 + 10 Torr Ar. The result of this crucial experiment is shown in Fig. 16. Again, N_2 and N_2O are produced, but the *isotopically mixed molecule* $^{14}N^{15}N$ is the

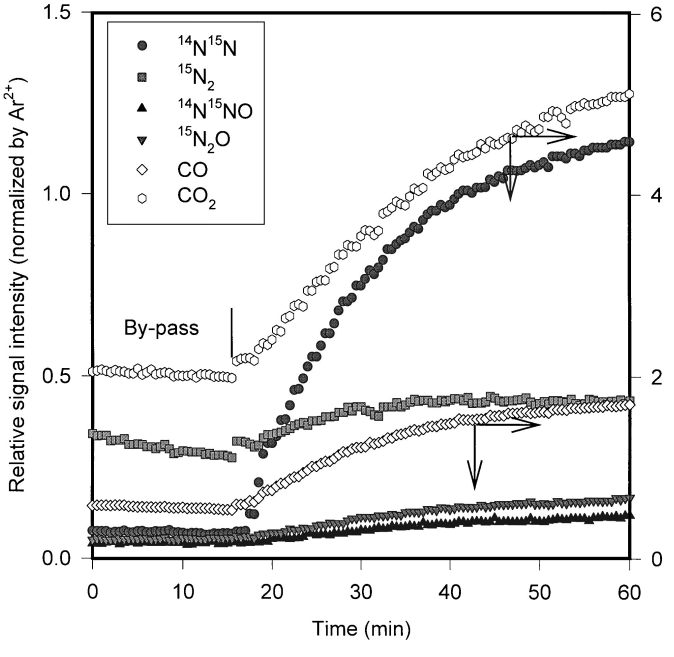

FIG. 16. Time dependence of the relative signal intensity upon circulating a mixture of 10 Torr ^{15}NO + 80 Torr O_2 + 10 Torr Ar over an Fe/ZSM-5 sample, on which a ^{14}N-containing deposit has been formed with i-C_4H_{10}.

predominant N-containing gas phase product. Small amounts of $^{15}N_2$ and $^{15}N_2O$ are also observed, but only in quantities similar to those obtained with the synthetic nitrogen-free deposit in Figure 15. A very small amount of isotopically mixed $^{14}N^{15}NO$ is also measured; its intensity is even lower than that of $^{15}N_2O$. The intensive signal at $M/e = 28$ is due to the formation of CO rather than $^{14}N_2$. Clearly, oxidation of the nitrogen-containing deposit results in the formation of CO and CO_2, in addition to N_2 and H_2O.

These results show that the nitrogen-containing deposit is highly reactive toward NO_2 (or $NO + O_2$), while it is much less reactive toward NO alone. As can be seen from Fig. 15 (open symbols), much less $^{15}N_2$ and only negligible amounts of $^{15}N_2O$ are formed with NO only. This is consistent with the FTIR results.

4. DISCUSSION

Dioxygen has been found to be crucial for the SCR of NO with NH_3 or hydrocarbon reductants over various catalysts (11). The present work shows that this is also true for the Fe/ZSM-5 catalyst. Oxygen reacts swiftly with NO to form NO_2, which then interacts with the catalyst to form chemisorption complexes of the type NO_y where $y \geq 2$. This is basically the same chemistry as that shown previously for other ZSM-5 supported metals (42). In the case of Cu/ZSM-5 there is good evidence that $[Cu–O–Cu]^{2+}$ ions are the active sites for NO oxidation to NO_2 (43). It is possible that $[HO–Fe–O–Fe–OH]^{2+}$ ions (4, 5) fulfill the same task in Fe/ZSM-5. An additional beneficial effect of oxygen is *in situ* removal of excessive carbonaceous deposits (44).

The present results show that strongly adsorbed NO_y complexes are formed on the Fe/ZSM-5 catalyst only if NO_2 is fed or when NO_2 is formed *in situ* from $NO + O_2$. The NO_y complexes are manifest from IR absorption bands at 1625 and 1570 cm^{-1}, which are similar to those observed by Adelman *et al*. over Cu/ZSM-5 (1628, 1594, 1572 cm^{-1}) (7). There is some debate on the assignment of these bands. Adelman *et al*. assigned the 1628 cm^{-1} band to a nitro group, while bands at 1594 and 1572 cm^{-1} were assumed to be caused by nitrate groups. Other researchers observing similar bands over Cu/ZSM-5 (45) assigned them to different kinds of nitrate ions. The main argument for the latter assignment is that the stability of the 1628 cm^{-1} is not easily reconciled with the assumption of a nitro group. However, assignment to a nitrate ion is also objectionable, since Adelman *et al*. did not observe a band at 1628 cm^{-1} after impregnation SiO_2 or Na/ZSM-5 with $Cu(NO_3)_2$. The bands appeared only upon heating the Na/ZSM-5-supported sample to 100°C, at which temperature the nitrate started to decompose. London *et al*. (46) studied the adsorption of NO_2 on copper oxide. They did not observe this band. Logan *et al*. (47) showed that both the α- and β-forms of copper (II) nitrate show bands below 1600 cm^{-1}. Therefore, we prefer to assign the 1628 cm^{-1} band to a nitro group, because its frequency is nearly the same as that of gas phase NO_2. The high thermal stability of this group on Cu/ZSM-5 may be due to the unique zeolite structure of ZSM-5. Still, we use the cautious term nitro/nitrate in this paper. A band at 1605 cm^{-1} was observed over NO_2 adsorbed α-Fe_2O_3, and it has been assigned to adsorbed nitro group (25). Considering these facts, we tentatively assign the band at 1625 cm^{-1} on $(NO + O_2)$ laden Fe/ZSM-5 as a nitro group, while assigning the band at 1570 cm^{-1} as a nitrate group at an iron site. These nitro/nitrate groups are stable at 200°C upon purging with He, as shown in Figs. 6 and 7. At higher temperature, they will decompose forming NO, NO_2, and O_2, as shown by the TPD profiles in Fig. 6.

These nitro/nitrate groups are potential reaction intermediates (7, 48). They show high reactivity toward hydrocarbons (see Figs. 8 and 9). In reacting with these groups, *iso*-butane is more active than propane. With *iso*-butane, the nitro/nitrate groups were virtually consumed within 5 min, while it took about 30 min when propane was used. This is in agreement with the proposed reaction mechanism for SCR of NO with hydrocarbons; i.e., the difficult, possibly rate limiting step in the reduction of NO with alkane is the rupture of the first C–H bond (6, 49–52). It is obvious that this C–H bond fission is much easier with *iso*-butane than with propane, since *iso*-butane, unlike propane, has a tertiary C–H bond.

Over Cu/ZSM-5, Adelman *et al*. (7) showed that the nitro/nitrate groups are inactive toward CH_4. Over Fe/ZSM-5, displaying the same bands, the same lack of activity toward methane is found in the present work.

The reaction between hydrocarbon and nitro/nitrate groups will lead to the formation of organic nitroso and/or nitro complexes, as has been proposed before (8, 37, 53, 54). Organic nitro compounds have very strong IR bands at about 1550 cm^{-1} and 1385–1365 cm^{-1}, while nitroso compounds absorb at 1590–1540 cm^{-1} (33). In the 1700–1300 cm^{-1} region, complicated absorption bands appear in Figs. 6, 7, and 10. Presumably, they will contain contributions from such organic nitroso and/or nitro compounds.

Nitroso compounds can easily undergo spontaneous isomerization to oximes. Over Cu/ZSM-5, Beutel *et al*. (8) found that ^{14}N-labeled acetone oxime readily reacts with ^{15}NO, forming $^{14}N^{15}N$ and $^{14}N^{15}NO$. They propose that this might be a reaction path in SCR of NO_x. The results in Figs. 8 and 13 confirm that this hypothesis is also valid for Fe/ZSM-5. When C_3H_8 was used as the reductant, 2-nitroso-(or nitro-)propane might be formed, which readily isomerizes to its oxime. This oxime and/or its hydrolysis compounds could further react with NO_2, forming N_2, N_2O, CO, CO_2, and H_2O. Therefore, when the NO_y-adsorbed sample is first exposed to the $C_3H_8 + O_2$ flow, an attenuation of the IR

bands corresponding to the nitro/nitrate groups is observed (see Fig. 8). Simultaneous release of N_2 and N_2O is found (see Fig. 13). Later, the amount of NO_y decreases, the process leading to N_2 formation is suppressed by lack of NO_2. Instead nitrogen-containing organic deposits are formed on the catalyst (see Fig. 8d). This deposit is stable against O_2 at 200°C, but is active toward NO_2 (or $NO + O_2$ when reaction (3) occurs) as shown in Figs. 10 and 14. NO_2 reacts quickly with the deposit forming N_2 and some N_2O.

Reaction of *iso*-butane with the nitro/nitrate groups has to result in different products. While initially tertiary nitroso and/or nitro compounds will be formed, these molecules cannot isomerize easily because there is no H atom in the α-position to the NO group. Instead of forming an oxime, these molecules apparently polymerize to a nitrogen-containing deposit on the catalyst. Very little N_2 or N_2O is released in this process (see Figs. 9 and 13). However, the most exciting finding of the present research is that this deposit is highly reactive toward NO_2. This reaction leads to the formation of gaseous N_2. Formation of an active nitrogen-containing organic intermediate when C_3H_6 was used as a reductant has been reported by Yogo *et al*. over H–Fe–silicalite (55) and by Guyon *et al*. over Cu/ZSM-5 (56). Both works show that N_2 is formed upon exposing the intermediate to NO_2. The present work with labeled molecules unambiguously shows that $^{14}N^{15}N$ is the predominant product, indicating that the two nitrogen atoms have different histories; i.e., one nitrogen atom comes from the deposit, while the other one comes from the gas phase NO_2.

Details of this reaction are still unclear. The deposit may undergo several reactions, such as oxidation, hydrolysis, and isomerization. Isocyanates and organic nitriles, and possibly also cyanates, appear as plausible groups from the FTIR spectra in Fig. 12. These intermediates have been claimed to be active in NO reduction (34–41). One can also speculate that hydroxylamine is formed upon hydrolysis. One hundred years ago, it was shown by Haber that nitrobenzene reacts with hydroxylamine to form azo-benzene (57); azo and diazo compounds are, of course, easily decomposed, releasing N_2. Formation of diazonium or diazo compounds would also be conceivable if the deposit contains amine groups, which react with HONO or N_2O_3 (58). HONO can be easily formed by the reaction

$$RH + NO_2 \rightarrow R\cdot + HONO. \qquad [4]$$

This possibility seems to be supported by the fact that only NO_2, and not NO or O_2, reacts quickly with the deposit. While this part is still speculative, the present results leave little doubt that interaction of NO_2 with the N-containing deposit formed from *iso*-C_4H_{10} and adsorbed nitro/nitrate complexes is a very efficient step in the reduction of NO_x to N_2 by this hydrocarbon.

The amount of N_2O released upon circulating $NO + O_2$ over the deposit-covered sample is nearly identical, regardless of whether the deposit is a nitrogen-containing or nitrogen-free complex, although the amount of N_2 formed is markedly different (compare the open plots in Fig. 14 and the solid plots in Fig. 15). Also, in the labeled experiment, less mixed $^{14}N^{15}NO$ than isotopically pure $^{15}N_2O$ is observed, in contrast to the predominance of the isotopically mixed $^{14}N^{15}N$ in Fig. 16. These results indicate that N_2O is presumably not an intermediate in the formation of N_2.

While the nitrogen-containing deposit is crucial for the SCR of NO_x, its accumulation may also block the sites for NO adsorption, as shown in Fig. 12. Therefore, the overall SCR activity depends, in a rather precarious way, on the amount of such deposits in the steady state. Suppression of NO oxidation to NO_2 by site blocking with deposit appears to be the easiest rationalization of the nontrivial dependence of the SCR rate on the nature of the hydrocarbon, shown in Fig. 2. Also, the temperature dependence of the relative effectiveness of the reductants between propane and *iso*-butane can be rationalized. At low temperature, the N_2 yield is lower with *iso*-C_4H_{10} than with C_3H_8, because more deposit is formed with *iso*-C_4H_{10}. At higher temperature, when the excess deposit (or its remainder after N_2 evolution) is burnt off, the reactivity sequence of these hydrocarbons is reversed and *iso*-C_4H_{10} is the better reductant. The same reasoning holds true for C_3H_6, which forms more coke on the catalyst, giving a lower N_2 yield as a result. Propene has been reported to be less effective than propane also over Cu/ZSM-5 (44, 59).

With propane as the reductant, the catalyst surface remains rather "clean," as follows from the FTIR spectra (Fig. 11) and the TPO result. Mononitrosyl, nitro/nitrate groups and carbonates are identified on the catalyst. This suggests that with propane the rate limiting step may be the C–H bond rupture. The equilibrium between NO and NO_2 remains established and, consequently, the N_2 yield does not change upon replacing NO with NO_2. With *iso*-C_4H_{10} as the reductant, the N_2 yield is higher with NO_2 than with NO, because the sites which catalyze the NO oxidation are, in part, blocked.

Addition of water vapor to the feed is known to suppress the formation of carbonaceous deposits (60). CO is formed in the reaction between the deposit and H_2O (4, 5). The present results show that addition of 10% H_2O to the *iso*-$C_4H_{10} + NO + O_2$ feed enhances the SCR activity at low temperature. No such effect was found for a $C_3H_8 + NO + O_2$ feed, in accordance with the fact that this gas leaves the catalyst surface rather "clean." Instead, H_2O will compete with NO for the iron sites or interfere with the oxidation of NO to form NO_y. These actions lead to a slight decrease in the activity. However, these adverse effects are,

fortunately, very small for the Fe/ZSM-5 catalyst in contrast to Cu/ZSM-5 and other catalysts (4).

5. CONCLUSIONS

Fe/ZSM-5 catalysts prepared via sublimation are active for the reduction of NO_x to N_2 with hydrocarbons such as propane, *iso*-butane, or propene, but not with methane. They remain active in the presence of a large excess of H_2O. The NO_x reduction rate is negligible in the absence of O_2; it increases steeply with increasing O_2 content of the feed and passes through a maximum. The equilibrium between $NO + O_2$ and NO_2 is swiftly established over a clean catalyst, but formation of deposits impedes this reaction. The formation of N_2 appears to be a multistep process. First, $NO + O_2$ form chemisorption complexes of the general type NO_y, with $y \geq 2$. These react with the hydrocarbon and, dependent on the chemical nature of this hydrocarbon, a deposit may be formed on the catalyst containing C, O, H, and N atoms. An intensive formation of N_2 is observed when NO_2 reacts with such a deposit, in particular if the latter was created from *iso*-C_4H_{10}. Isotopic labeling shows that one N atom in every N_2 molecule formed in this step comes from the deposit, while the other comes from NO_2. N_2O is not a precursor of N_2. The intermediate formation of a diazo complex is suggested. Deposits can also block catalyst sites, including those needed for the NO oxidation to NO_2. The rate limiting step, therefore, depends on the nature of the hydrocarbon used and the type and quantity of the deposit. As deposits are oxidized by O_2 and volatilized by H_2O at high temperature, the relative efficiency of different hydrocarbons in NO_x reduction over Fe/ZSM-5 depends on the temperature and the H_2O content of the feed.

ACKNOWLEDGMENTS

Financial support for this research by an unrestricted grant from the Ford Motor Corporation is gratefully acknowledged. We thank Dr. Steve Wilson of UOP, Dr. Arno Tißler of ALSI-Penta Zeolithe GmbH, Dr. Karin Bartels of Degussa, and Dr. Armin Pfenninger of Uetikon Chemie A.G. for kindly donating ZSM-5 samples.

REFERENCES

1. Feng, X., and Hall, W. K., *Catal. Lett.* **41**, 45 (1996).
2. Feng, X., and Hall, W. K., *J. Catal.* **166**, 368 (1997).
3. Sachtler, W. M. H., and Chen, H.-Y., U.S patent pending, Appl. No. 60/052,382 (1997).
4. Chen, H.-Y., and Sachtler, W. M. H., *Catal. Today* **42**, 73 (1998).
5. Chen, H.-Y., and Sachtler, W. M. H., *Catal. Lett.* **50**, 125 (1998).
6. Cowan, A. D., Dümpelmann, R., and Cant, N. W., *J. Catal.* **151**, 356 (1995).
7. Adelman, B. J., Beutel, T., Lei, G.-D., and Sachtler, W. M. H., *J. Catal.* **158**, 327 (1996).
8. Beutel, T., Adelman, B. J., and Sachtler, W. M. H., *Catal. Lett.* **37**, 125 (1996).
9. Walker, A. P., *Catal. Today* **26**, 107 (1995).
10. Adelman, B. J., Lei, G.-D., and Sachtler, W. M. H., *Catal. Lett.* **28**, 119 (1994).
11. Shelef, M., *Chem. Rev.* **95**, 209 (1995).
12. Fritz, A., and Pitchon, V., *Appl. Catal. B* **13**, 1 (1997).
13. Iwamoto, M., and Mizuno, N., *Proc. Inst. Mech. Eng. D* **207**, 23 (1992).
14. Chajar, I., Primet, M., Praliaud, H., Chevrier, M., Gauthier, G., and Mathis, F., *Catal. Lett.* **28**, 33 (1994).
15. Petunchi, J. O., Sill, G., and Hall, W. K., *Appl. Catal. B* **2**, 303 (1993).
16. Schay, Z., and Guczi, L., *Catal. Today.* **17**, 175 (1993).
17. Chang, Y. F., and McCarty, J. G., *J. Catal.* **165**, 1 (1997).
18. Matyshak, V. A., Ilichev, A. N., Ukharsky, A. A., and Korchak, V. N., *J. Catal.* **171**, 245 (1997).
19. Corna, A., and Massot, R. (Eds.), "Compilation of Mass Spectroscopy Data." Heyden, London, 1966.
20. Chao, C. C., and Lunsford, J. H., *J. Am. Chem. Soc.* **93**, 71 (1971).
21. Teranishi, R., and Decius, J. C., *J. Chem. Phys.* **22**, 896 (1954).
22. Hoost, T. E., Laframboise, K. A., and Otto, K., *Catal. Lett.* **33**, 105 (1995).
23. Szanyi, J., and Paffett, M. T., *J. Catal.* **164**, 232 (1996).
24. Hadjiivanov, K., Saussey, J., Freysz, J. L., and Lavalley, J. C., *Catal. Lett.* **52**, 103 (1998).
25. Busca, G., and Lorenzelli, V., *J. Catal.* **72**, 303 (1981).
26. Aparicio, L. M., Hall, W. K., Fang, S.-M., Ulla, M. A., Millman, W. S., and Dumesic, J. A., *J. Catal.* **108**, 233 (1987).
27. Amiridis, M. D., Puglisi, F., Dumesic, J. A., Millman, W. S., and Topsøe, N.-Y., *J. Catal.* **142**, 572 (1993).
28. Nakamoto, K., "Infrared Spectra of Inorganic and Coordination Compounds" (3rd ed.), p. 109. Wiley, New York, 1978.
29. Valyon, J., and Hall, W. K., *J. Phys. Chem.* **97**, 1204 (1993).
30. Rochester, C. H., and Topham, S. A., *J. Chem. Soc. Faraday Trans. 1* **75**, 872 (1979).
31. Segawa, K.-I., Chen, Y., Kubsh, J. E., Delgass, W. N., Dumesic, J. A., and Hall, W. K., *J. Catal.* **76**, 112 (1982).
32. Guglielminotti, E., *J. Phys. Chem.* **98**, 9033 (1994).
33. Socrates, G., "Infrared Characteristic Group Frequencies" (2nd ed.). Wiley, New York, 1994.
34. Bell, V. A., Feeley, J. S., Deeba, M., and Farrauto, R. J., *Catal. Lett.* **29**, 15 (1994).
35. Hayes, N. W., Grünert, W., Hutchings, G. J., Joyner, R. W., and Shpiro, E. S., *J. Chem. Soc. Chem. Commun.*, 531 (1994).
36. Hayes, N. W., Joyner, R. W., and Shpiro, E. S., *Appl. Catal. B* **8**, 343 (1996).
37. Yokoyama, C., and Misono, M., *J. Catal.* **150**, 9 (1994).
38. Radtke, F., Koeppel, R. A., and Baiker, A., *J. Chem. Soc. Chem. Commun.*, 427 (1995).
39. Radtke, F., Koeppel, R. A., Minardi, E., and Baiker, A., *J. Catal.* **167**, 127 (1997).
40. Li, C., Bethke, K. A., Kung, H. H., and Kung, M. C., *J. Chem. Soc. Chem. Commun.*, 813 (1995).
41. Aylor, A. W., Lobree, L. J., Reimer, J. A., and Bell, A. T., *Stud. Surf. Sci. Catal.* **101**, 661 (1996).
42. Hamada, H., Kintaichi, U., Sasaki, M., and Ito, T., *Appl. Catal.* **70**, L15 (1991).
43. Lei, G.-D., Adelman, B. J., Sárkány, J., and Sachtler W. M. H., *Appl. Catal. B* **5**, 245 (1995).
44. d'Itri, J. L., and Sachtler, W. M. H., *Appl. Catal. B* **2**, L7 (1993).
45. Hadjiivanov, K., Klissurski, D., Ramis, G., and Basca, G., *Appl. Catal. B* **7**, 251 (1996).
46. London, J. W., and Bell, A. T., *J. Catal.* **31**, 32 (1973).
47. Logan, N., and Simpson, W. B., *Spectrochim. Acta* **21**, 857 (1965).
48. Beutel, T., Adelman, B. J., Lei, G.-D., and Sachtler, W. M. H., *Catal. Lett.* **32**, 83 (1995).
49. Adelman, B. J., Beutel, T., Lei, G.-D., and Sachtler, W. M. H., *Appl. Catal. B* **11**, L1 (1996).

50. Witzel, F., Sill, G. A., and Hall, W. K., *J. Catal.* **149**, 229 (1994).
51. Lukyanov, D. B., Sill, G., d'Itri, J. L., and Hall, W. K., *J. Catal.* **153**, 265 (1995).
52. Li, Y., and Armor, J. N., *J. Catal.* **150**, 376 (1994).
53. Li, Y., Slager, T. L., and Armor, J. N., *J. Catal.* **150**, 388 (1994).
54. Lombardo, E. A., Sill, G. A., d'Itri, J. L., and Hall, W. K., *J. Catal.* **173**, 440 (1998).
55. Yogo, K., Ono, T., Ogura, M., and Kikuchi, E., *in* "Reduction of Nitrogen Oxide Emission" (U. S. Ozkan, S. K. Agarwal, and G. Marcelin, Eds.), p. 123. ACS, Washington, DC, 1995.
56. Guyon, M., Chanu, V. Le., Gilot, P., Kessler, H., and Prado, G., *Appl. Catal. B* **8**, 183 (1996).
57. Haber, F., *Z. Elektrochem.*, 506 (1898).
58. March, J., "Advanced Organic Chemistry: Reactions, Mechanisms, and Structure" (2nd Ed.), p. 578. McGraw–Hill, New York, 1977.
59. Gaudin, C., Duprez, D., Mabilon, G., and Prigent, M., *J. Catal.* **160**, 10 (1996).
60. Kharas, K. C. C., Robota, H. J., and Liu, D. J., *in* "AIChE Symposium," Paper No. 240b. Miami Beach, FL, Nov. 1992.